International Journal of Heat and Mass Transfer 255 (2026) 127813

Contents lists available at ScienceDirect

International Journal of Heat and Mass Transfer

journal homepage: www.elsevier.com/locate/ijhmt

Stable implementation of a Chen-based enhancement to the Lee phase-change model for CFD simulation of film boiling under energetic melt-coolant interaction conditions

Mihael Boštjan Končar [a,b,*], Matej Tekavčič [b], Mitja Uršič [b,c], Mihael Sekavčnik [a]

[a] Faculty of Mechanical Engineering, University of Ljubljana, Aškerčeva cesta 6, SI-1000 Ljubljana, Slovenia
[b] Jožef Stefan Institute, Jamova cesta 39, SI-1000 Ljubljana, Slovenia
[c] Faculty of Mathematics and Physics, University of Ljubljana, Jadranska ulica 19, SI-1000, Ljubljana, Slovenia

ARTICLE INFO

Keywords:
Heat transfer
Film boiling
Extreme thermal conditions
Phase-change modelling
Computational fluid dynamics (CFD)
Two-phase flow

ABSTRACT

This study investigates heat and mass transfer during energetic melt-coolant interactions, focusing on film boiling around a hot melt particle in subcooled convective flow. The considered conditions, free-flow velocities of a few m/s, melt particle temperatures of several thousand K, particle diameters of several tens of a μm, and liquid subcooling of several tens of a K, align with TREPAM experiments (CEA, France).

A two-phase computational fluid dynamics framework, based on the Volume of Fluid method, is used. An improved phase-change model is implemented, combining Chen's explicit formulation of the phase-change intensity factor with the robustness of the conventional Lee model. The approach reduces sensitivity to empirical parameters and enhances phase-change localisation. Additional constraints on the intensity factor ensure numerical stability under extreme thermal conditions relevant to vapour energetic melt-coolant interactions.

Simulations of TREPAM experiments demonstrate improved heat flux predictions and enhanced flow dynamics capture. Analysis of the simulated velocity fields reveal secondary flows in the vapour wake, impacting heat and mass transfer and emphasizing the need to resolve vapor-phase flow conditions. To fully validate proposed modifications to phase-change model further numerical and experimental investigation is required, focusing on vapour film morphology and localized heat transfer intensity.

1. Introduction

Efficient cooling via energy-intensive phase change is important in many advanced technologies. However, film boiling disrupts effective cooling and even damage technological equipment. This phenomenon is particularly relevant to the nuclear safety during severe accidents, where film boiling inhibits quenching of molten reactor material and increases the risk of vapour explosions. Studies of this phenomena have been going on for several decades, both for current light-water-cooled thermal reactors, as well as for future innovative sodium-cooled fast reactors [1–3]. Further, film boiling has been studied in relation to accident-tolerant fuel behaviour under reflooding conditions [4]. Beyond nuclear applications, film boiling is relevant for quenching of high-temperature industrial surfaces such as steel [5] and addressing the hazards of liquefied natural gas spillages on water [6]. It also plays a key role in geophysical phenomena, such as defining magma cooling rates during phreatomagmatic and submarine eruptions, which influence transitions between explosive and non-explosive magma fragmentation [7]. Due to its widespread significance, extensive experimental, theoretical, and computational studies have been conducted to understand how coolant properties (thermodynamic conditions, velocity, temperature), surface characteristics (geometry, material, orientation, temperature), and ambient pressure affect heat transfer intensity of film boiling. For example, several numerical and experimental studies on film boiling in forced convection water flow have been conducted [8–13], but only a few refer to the extreme conditions observed prior to and during vapour explosions [10,14,15].

In this context, it is important to clarify what is meant by extreme conditions, as referred to in the present work. These conditions are characteristic of the vapour explosions and are defined by the presence of at least one of the following:

* Corresponding author.
E-mail address: MihaelBostjan.Koncar@fs.uni-lj.si (M.B. Končar).

https://doi.org/10.1016/j.ijheatmasstransfer.2025.127813
Received 3 March 2025; Received in revised form 30 July 2025; Accepted 7 September 2025
Available online 12 September 2025

Nomenclature

Symbols

A	area, [m^2]
c	specific heat capacity, [J/(kg K)]
D	diameter, [m]
e	specific energy, [J/kg]
f	frequency, [s^{-1}]
$\boldsymbol{f}$	volumetric force, [N/m^3]
g	gravitational acceleration, [m/s^2]
h	mass specific enthalpy, [J/kg]
k	heat conductivity, [J/(kg K)]
$\dot{m}$	mass flow rate, [kg/s]
p	pressure, [Pa]
q	heat flux, [W/m^2]
$\dot{Q}$	heat transfer rate, [W]
r	mass transfer intensity factor, [s^{-1}]
Re	Reynolds number, [-]
S	source term, [kg/(s m^3)] or [W/m^3]
St	Strouhal number, [-]
t	time, [s]
T	temperature, [K]
U	velocity, [m/s]
$\boldsymbol{v}$	velocity (vector), [m/s]
V	volume,[m^3]
We	Weber number, [-]
δ	thickness, [m]
Δx	cell length, [m]
μ	dynamic viscosity, [Pa s]
ρ	density, [kg/m^3]
σ	surface tension, [N/m]
$\boldsymbol{\tau}$	viscous stress tensor, [Pa]
ϕ	volume fraction, [-]

Indexes

∞	free flow
Chen	Chen's model
crit	critical
eff	effective
MPC	Modified Phase-Change model
exp	experimental
h	enthalpy
int	interfacial
L	liquid
Lee	Lee's model
LV	liquid to vapour
max	maximal
sat	saturation
surf	surface
T	turbulent
V	vapour
w	wall
Δ	representative volume
q	heat flux
r	relative
s	shedding
σ	relating to surface tension effects

- surface temperatures significantly exceeding both the Leidenfrost and critical temperatures;
- large subcooling of the coolant, such that the available thermal energy cannot be entirely consumed for interfacial phase change, leading to rapid condensation and pressure transients;
- large coolant flow velocities, sufficient to induce forced convection effects and the potential disintegration of liquid structures; and
- ambient pressures approaching or exceeding the critical pressure of the fluid.

These conditions contribute to complex two-phase flow dynamics and introduce substantial non-linearities in the governing transport processes, which pose challenges for both numerical modelling and experimental measurement.

One of the most common used methods for modelling heat transfer during film boiling in nuclear engineering is the Epstein-Hauser Correlation (EHC) [13]. It is implemented in multi-fluid models such as MC3D [16] and IDEMO [17], which predict the integral effects of energetic thermal interactions between fuel and coolant in complex multiphase systems occurring in reactor vessels and containment cavities. The EHC correlation is a physically based method that considers fluid properties but requires experimental calibration [13]. However, under extreme conditions its accuracy is assessed to be around 75 % [18]. One of the probable reasons for this limitation is the assumption of a smooth liquid-vapor interface in boundary layer analyses [13], which neglects complex and dynamic behaviour of two-phase flows under such conditions.

To overcome these limitations, computational fluid dynamics (CFD) simulations can provide a detailed and flexible approach, offering insight into liquid-vapor interface morphology and enabling the analysis of critical parameters, such as vapour film velocity, mass transfer intensity, and phase-change location. Further, CFD simulations can capture phenomena that are otherwise inaccessible by experimental methods, enhancing the understanding of film boiling dynamics under extreme conditions. Furthermore, CFD-based studies also allow the investigation of heat transfer mechanisms in coolants that are challenging to study experimentally due to their physical properties such as opacity and reactivity. This capability is particularly significant for advancing the understanding of heat transfer phenomena in coolants like sodium and lead, which are used in advanced fast-neutron nuclear reactors (Generation IV). The CFD results can thus support the development of generalised correlations and guide future experimental work.

Evidently, for the stated purposes, approaches to modelling boiling in CFD codes are important. They can be generally classified into four main categories, which are briefly summarised below in the context of our simulation. Detailed descriptions of each category are provided in [19].

i. **Rankine-Hugoniot energy jump condition-based models** [20]: This approach models energy transfer across the liquid-vapor interface, incorporating heat conduction in both phases. It is physically grounded and avoids empirical parameters but neglects contributions from kinetic energy. While this method is suitable for simple phase-change scenarios, it is limited to mass transfer strictly at the interface, making it unsuitable for more complex situations like subcooled inlet boiling or cases without a pre-existing interface.
ii. **Schrage based models** [21]: Derived from the kinetic theory of gases, this approach assumes that both the liquid and vapour phases are in saturation state but allows for temperature and pressure discontinuities across the interface. This model provides a physical basis for including kinetic energy effects, but its accuracy is highly dependent on the determination of the accommodation coefficient, which is challenging to measure experimentally or predict theoretically.

iii. **Lee based models** [22]: A simplified approach, assuming that phase change is driven by the temperature deviation from the saturation conditions. Its versatility and ease of implementation have made it a common choice in CFD simulations. However, the reliance on an empirical mass transfer intensity factor and its tendency to enforce saturation conditions limits its accuracy and physical fidelity, particularly under transient or extreme conditions.

iv. **Other Approaches**: Additional methods include those tailored to specific cases, and may consider Marangoni effects, pseudo-nucleate boiling, or use dedicated experimentally derived correlations [23–25]. These approaches are typically application-specific or necessitate significant computational power, which limit their general applicability.

In the context of CFD-based studies of film boiling heat transfer under extreme conditions relevant to vapour explosions, limited scientific work is available. This can largely be attributed to the numerical complexity of the problem, driven by large temperature gradients and strong non-linearities. Moreover, since vapour explosion phenomena have been relatively well investigated experimentally in water, CFD modelling has not historically been at the forefront of research efforts. However, this is now changing with the increasing interest in liquid metal coolants, where the development of robust CFD methods has become essential.

Nevertheless, some approaches have been proposed that model the two-phase system as a quasi-single-phase system [26], thereby restricting their applicability to supercritical conditions. Some studies have further suggested representing the vapour phase as a solid, effectively reducing the system to a quasi-single-phase framework [27].

A recent study [28] used a multiphase CFD approach with Chen's modifications [29] of the Lee phase-change model [22] to model larger melt droplet (several mm) fragmentation in low-velocity flows (<0.5 m/s). While methodologically related to approach proposed in this work, it focused on larger droplets and different (less extreme) thermal conditions.

This paper introduces a comparable but novel method for numerical modelling of the heat transfer around the melt fragment moving through subcooled liquid. The primary contribution is the development and justification of an enhanced phase change model adapted for simulating film boiling phenomena under extreme conditions, like those encountered in vapour explosions (large liquid subcooling, high melt temperatures, high relative flow velocity). The proposed model was first verified and validated against the analytical solution of the classical Stefan problem [30] and later compared with experimental data from the TREPAM facility (CEA, France) [14]. This study presents one of the first attempts to perform separate effect studies based on TREPAM experiments considering a fully two-phase flow CFD approach.

2. Flow conditions

Melt particle moving through coolant in premixing and explosive Fuel-Coolant Interaction (FCI) stages forms multiphase system with complex interactions between individual phases, including evaporation and condensation. Our primary goal is to study the film boiling in forced convection flow in extreme FCI conditions, expected to be observed during nuclear severe accidents resulting in reactor core material (corium) melting. Conditions of interests are [15,18]:

- extremely high particle surface temperatures (above 3000 K),
- significant liquid subcooling (over 10 K),
- particle velocities (relative to coolant flow) ranging from a few m/s (premixing stage) to several tens of m/s (explosion stage),
- pressures from about 0.1 MPa (premixing stage) to several tens MPa (explosion stage), and
- particle size ranging from few tens μm (explosion stage) to several mm (premixing stage) [31,32].

2.1. TREPAM experiments

Considering the outlined criteria, the water experiments from the TREPAM facility (CEA, France) [14] were chosen as a benchmark case. In the experiment, a melt particle is represented by an overheated tungsten wire moving at a constant velocity through the water (Fig. 1). In this configuration, the controlled (independent) parameters are the diameter (D), temperature of the wire (T_w), the water temperature (T_∞), and the wire velocity (U_∞). The setup also allows control of the operating pressure. The experimentally defined parameter is heat flux from the wire to the water (q_{exp}). Here, the radiative heat transfer is assumed to be negligible, due to the low value of tungsten emissivity (radiative contribution is at maximum 5 % of the measured heat flux) [14].

Due to the complexity and computational demands of the analysis (see Section 4), the presented study is limited to the TREPAM experimental cases [14] listed in Table 1. Based on similarity with the considered FCI conditions, case 54 was selected as a baseline case. Effects of T_w, D, U_∞ and T_∞ were investigated by comparison of cases 53, 61 and 55 against the baseline case (see Table 1). Operating pressure in all the listed cases is 0.12 MPa.

2.2. Analysis in support of numerical model development

Considered spatial scale of micrometres (μm) and a time scale of microseconds (μs) is consistent with the continuum assumption [33]. The effects of fluid compressibility could be neglected, as velocities exceeding 0.3 Mach were not expected. Additionally, several models used (see Section 3) are not adapted for the treatment of compressible flow.

An important advantage of the TREPAM experiment is tungsten's high thermal conductivity and small wire diameter, which ensures a Biot number well below 0.1. This justifies the assumption of a uniform temperature distribution within the particle volume, enabling the use of the Lumped Capacitance Method (LCM) [34] and simplifying the specification of boundary conditions on the particle surface.

Multiphase flow in the experiments can be characterised by the liquid (Re_L) and vapour (Re_V) Reynolds numbers:

$$Re_L = \frac{\rho_L U_\infty D}{\mu_L}, \quad Re_V = \frac{\rho_V U_\infty D}{\mu_V}, \tag{1}$$

where ρ represents density and μ dynamic viscosity of the fluid. The index L refers to liquid and V to vapour phase. The fluid properties are estimated at $T_L = \frac{T_\infty + T_{sat}}{2}$ and $T_V = \frac{T_w + T_{sat}}{2}$ for liquid and vapour phase, respectively [35].

In the flow around a cylinder the transition to turbulence occurs at Re numbers between 150 and 300 [36]. For selected experiments the considered Re_L numbers (see Table 1) describe the range from laminar to turbulent flow and include the transition region. This indicates that turbulence affect the multiphase flow and must be considered in the CFD

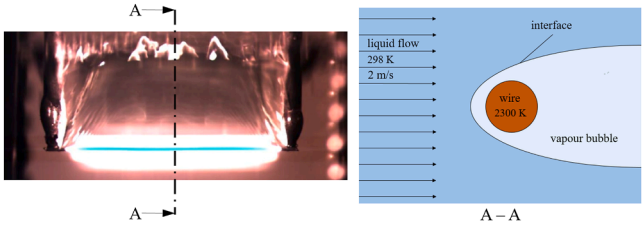

Fig. 1. Picture of the observed phenomenon in the experimental facility TREPAM [14] (left) and schematic representation (right).

Table 1
Detailed description of the simulated TREPAM cases [14]. Cases are compared to baseline case by quantities written in bold.

Case	$D[\mu m]$	$U_\infty \left[\frac{m}{s}\right]$	$T_w[K]$	$T_\infty[K]$	$T_{sat} - T_\infty[K]$	Re_L [/]	$q_{exp} \left[\frac{MW}{m^2}\right]$
54 (baseline)	96	2	2300	293	84	294	18
53	100	2	**1780**	294	83	312	14
55	99	2	1900	361	**16**	644	9
61	**47**	**0.2**	2300	303	74	17.2	16

model. Due to higher anticipated relative flow velocity during the realistic explosion stage in water, Re_L and Re_V are expected to be higher than observed in the selected experiments (Table 1). However, the Re in sodium is expected to match the experimental values [37] more closely.

The dynamic interaction between vapour and liquid phase is dictated by the effect of surface tension. For flows with high Re number this effect is evaluated by criterion based on Weber number [38,39], which represents the ratio between the drag force in the fluid and the cohesive forces:

$$\mathbf{We}_{\mathbf{crit}} = \frac{\boldsymbol{\rho}\ \boldsymbol{v}^2\ \boldsymbol{D}}{\boldsymbol{\sigma}}, \tag{2}$$

where ρ denotes the density of the liquid, v the average relative flow velocity, σ the surface tension coefficient, and D the characteristic diameter of the melt particles (the wire). Considering all flow conditions, the We number was estimated to be about 5. Thus, the influence of surface tension is not negligible, as the estimated We number only slightly differs from the critical value ($We_{crit} = 1$) [38,39]. It is also important to note that in the case of liquid sodium or similar metal, the effect of surface tension is further enhanced due to larger surface tension coefficient [38].

Finally, in all cases, buoyancy effects and gravity can be neglected due to the small geometry and high flow velocities, i.e., when $U_\infty > \sqrt{g\ D}$ [33,39].

3. Numerical model

The problem of multiphase system comprising melt particles, liquid, and vapour was reduced to an analysis of liquid-vapour flow, due to use of LCM method. The primary heat transfer mechanism between the superheated wire and the coolant (water) is forced convection film boiling [14–16,18].

3.1. Basic model setup

Our preliminary studies [40,41] have shown that the interface tracking is of great significance when simulating such physical processes. Namely, the thickness of vapour film in front of the melt particle has the highest impact on the wall heat flux [40,41]. Hence, a single-fluid approach to two-phase flow modelling was adopted, enabling the application of interface tracking methods. In the presented study the simulations were preformed using the implicit formulation of Volume of Fluid model (VOF) [42] with Sharp Interface Modelling in the ANSYS Fluent 2019 R3 [39]. The phase change modelling problem is thus primarily reduced to determining mass and energy source terms (S_V and S_h) in main governing equations for total energy conservation and phase transfer. Accordingly, the complete set of governing equations employed in the simulations is outlined below [39]:

- mass conservation equation:

$$\begin{aligned} &\frac{\partial \rho}{\partial t} + \nabla\cdot(\rho \boldsymbol{v}) = 0; \\ &\phi_L = 1 - \phi_V,\ \rho = \rho_L\ \phi_L + \rho_V\ \phi_V \end{aligned} \tag{3}$$

- momentum conservation equation:

$$\begin{aligned} &\frac{\partial}{\partial t}(\rho \boldsymbol{v}) + \nabla\cdot(\rho \boldsymbol{v}\boldsymbol{v}) = -\nabla p + \nabla\cdot((\mu + \mu_T)\nabla \boldsymbol{v}) + \frac{1}{3}\nabla[(\mu + \mu_T)(\nabla\cdot \boldsymbol{v})] + \rho \boldsymbol{g} + \boldsymbol{f}_\sigma; \\ &\mu = \mu_L\ \phi_L + \mu_V\ \phi_V \end{aligned} \tag{4}$$

- total energy conservation equation:

$$\begin{aligned} &\frac{\partial}{\partial t}(\rho\ e) + \nabla\cdot[\boldsymbol{v}(\rho\ e + p)] = \nabla\cdot\left[k_{eff}\nabla T + \left(\boldsymbol{\tau}_{eff}\cdot \boldsymbol{v}\right)\right] + S_h; \\ &e = \frac{e_L\ \rho_L\ \phi_L + \ e_V\ \rho_V\ \phi_V}{\rho_L\ \phi_L + \rho_V\ \phi_V}, \\ &e_L = h_L - \frac{P}{\rho_L} + \frac{v^2}{2},\ \text{same for phase } V, \\ &h_L = c_{p,L}(T - T_{sat}),\ \text{same for phase } V, \end{aligned} \tag{5}$$

- phase transfer equation:

$$\frac{\partial}{\partial t}\rho_L\phi_L + \nabla\cdot(\rho_L\phi_L \boldsymbol{v}) = S_L = -S_V. \tag{6}$$

In the equations, $\boldsymbol{v}$ represents the velocity vector field, ρ density, ϕ the phase volume fraction, p pressure, μ dynamic viscosity, $\boldsymbol{g}$ gravitational acceleration, e the total energy, h the specific enthalpy, k_{eff} the effective thermal conductivity (including the effects of turbulence), $\boldsymbol{\tau}_{eff}$ the tensor of viscous stresses (viscous heat dissipation), and c_p the specific heat at constant pressure. Indexes L and V correspond to liquid and vapour phase, respectively. The turbulent viscosity μ_T accounts for the effects of turbulence and is obtained from the k-ω Shear Stress Transport (SST) turbulence model [43], while the volumetric force $\boldsymbol{f}_\sigma$ represents interfacial dynamic effects due to surface tension and is derived from the Continuum Surface Force model (CSF) [44].

The selection of the turbulence model was based on non-dimensional analysis, prior experience, model capabilities, and mesh characteristics. The computational mesh exhibits strong gradients in cell size, characterised by fine resolution near the heated surface and coarser cells in the bulk region. This requires a turbulence model capable of accurately

capturing near-wall behaviour while remaining effective in less resolved free-flow regions. The k–ω SST model was therefore selected due to its robustness and its ability to blend the k–ω formulation, which performs well with fine near-wall meshes, with the k–ε formulation, which is better suited for modelling turbulence in the free-flow on coarse grids [43].

Additionally, the fine near-wall mesh required by the VOF method ensures that the non-dimensional wall distance y^+ remains well below 1, fully satisfying the SST model's resolution requirements [39].

It should be noted that most turbulence models, including the k–ω SST model, are not specifically calibrated for multiphase flows and therefore introduce a degree of modelling uncertainty. Nevertheless, the k–ω SST model remains one of the most extensively studied and commonly applied Unsteady Reynolds Averaged Navier-Stokes (URANS) approaches in multiphase flow simulations [19].

3.2. Modifications to the phase-change model

Based on the aforementioned research (see section 1) and our preliminary studies [30,40], the phase-change model was identified as the most influential parameter in detailed CFD simulations. For the purpose of our studies the phase-change model shall correspond to the following criteria:

- versatile enough to be applicable to several coolants (e.g., water, sodium);
- formulated on a physical basis, thereby eliminating the need for numerical correction factors;
- capable of maintaining a distinct interface between liquid and vapour phases;
- precise in pinpointing the locations within the domain where boiling occurs;
- numerically feasible to simulate extreme conditions (subcooling > 50 K, wall temperature > 2000 K)
- capable of withstanding large gradients in temperature and density, which lead to significant source terms in the partial differential equations.

Due to its simplicity and widely use in commercial CFD software [19,29,45], the Lee Evaporation-Condensation Model [22] was chosen as the starting point for this study This model is also relatively straight-forward to implement in CFD software.

In the Lee model the intensity of the phase change is assumed to be proportional to the temperature difference between the temperature T in the computational cell and the saturation temperature T_{sat}. The source term is thus defined as [22]:

$$S_V = \begin{cases} r_{Lee}\ \phi_L\ \rho_L \dfrac{T - T_{sat}}{T_{sat}}; T > T_{sat} : \text{evaporation} \\ r_{Lee}\ \phi_V\ \rho_V \dfrac{T - T_{sat}}{T_{sat}}; T < T_{sat} : \text{condensation} \end{cases}. \quad (7)$$

In the equation, the empirical mass transfer intensity factor, r_{Lee}, with the unit $[s^{-1}]$, is used to ensure convergence of calculations. Generally, r_{Lee} can vary for evaporation and condensation processes, but it is common practice to use the same value for both processes [22].

The energy source term S_h is defined as the latent heat released upon phase change [22]:

$$S_h = -S_V\ h_{LV}, \quad (8)$$

where h_{LV} represents specific latent heat.

In preliminary study [40], we evaluated the Lee model for simulations of film boiling around a cylinder in subcooled liquid flow. It was observed in [29,40,45] that the outcomes of simulations highly dependents on the value of r_{Lee}. An inappropriate choice of r_{Lee} can lead to incorrect predictions, not only in terms of heat transfer intensity but also regarding the overall flow regime. Without experimental data specific to each case for model calibration, the accuracy of simulations remains questionable. This presents a significant challenge in simulations of phenomena in sodium, where, to the best of our knowledge, experimental data are unavailable for forced convection film boiling conditions. When dealing with large temperature gradients, typical in our case, the constant definition of r_{Lee} throughout the entire domain also poses a major deficiency.

To address the outlined challenges and modelling requirements, an improved phase-change modelling approach is proposed. For clarity, it is referred to as the Modified Phase-Change (MPC) model. The MPC model combines two well-established formulations: the physically based Chen model [29] and the numerically stable Lee model [22]. The Chen model is based on two main assumptions:

i. The interphase cell is adjacent to a cell fully filled with liquid. During the phase change process, the temperature of the liquid-filled cell equals the saturation temperature T_{sat}.
ii. The heat flux from the interphase cell to the adjacent liquid-filled cell drives the phase change process. The primary mechanism of heat transfer is conduction.

Fig. 2a presents a hypothetical scenario fitting the stated assumptions, and Fig. 2b shows the corresponding temperature profile in the discrete domain. In real simulations, the temperature in cell $i + 1$ may exceed T_{sat}.

For a simplified explanation of the Chen's model basic concept, phase change and fluid motion are disregarded, and the scenario is treated as heat conduction between two solids. The heat flux from the interfacial surface to cell $i + 1$ is examined. In this discrete domain analysis, the heat flux between the cell-centre I at temperature T and cell-centre $I + 1$ at temperature T_{sat} is considered. This heat flux in 1D can be described using Fourier's law [29]:

$$\dot{Q} = -k_L \frac{T - T_{sat}}{0,5\Delta x + 0,5\phi_L \Delta x} A_{int}, \quad (9)$$

where k_L and A_{int} represents the thermal conductivity of the liquid and the size of the interfacial area, respectively.

Consistent with the second assumption of Chen's model, it is assumed that in the case of phase transfer, the entire heat transfer rate $\dot{Q}$ goes to the phase change:

$$\dot{Q} = -h_{LV}\ \Delta \dot{m}_V. \quad (10)$$

The volumetric mass source S_V, can be then defined based on the

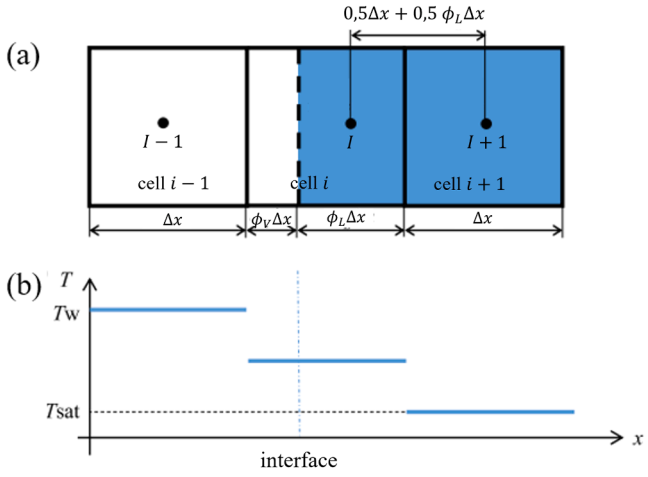

Fig. 2. Graphical representation of assumptions in Chen's model and the temperature profile in the discrete domain (adopted from [29]).

vapour mass source $\Delta\dot{m}_V$:

$$S_V = \frac{\Delta\dot{m}_V}{V_\Delta} = -\frac{\dot{Q}}{h_{LV}\ V_\Delta} = -k_L \frac{T - T_{sat}}{h_{LV}\ (0,5\Delta x + 0,5\phi_L \Delta x)} \frac{A_{int}}{V_\Delta}. \tag{11}$$

Following Lee's formulation of the evaporation model, Chen's model can be expressed as follows [29]:

$$S_V = r_{Chen}\ \phi_L\ \rho_L \frac{T - T_{sat}}{T_{sat}},$$

$$S_h = \ -h_{LV}\ S_V;$$

$$T > T_{sat},$$

$$r_{Chen} = \frac{k_L\ c_{p,L}\ T_{sat}}{\rho_L\ h_{LV}\ \Delta x\ (0,5 + 0,5\phi_L)} \frac{A_{int}}{V_\Delta}. \tag{12}$$

In this manner, the factor r_{Chen} is explicitly defined as a function of the fluid properties and computational grid parameters. Additionally, this factor is no longer constant throughout the entire domain, thereby achieving a more physically representation of the process.

In Eq. (11) and (12), the term $\frac{A_{int}}{V_\Delta}$ is referred to as the Interfacial Area Density (IAD). In 1D grid with uniform spacing Δx, IAD calculation is straightforward ($\frac{A_{int}}{V_\Delta} = \frac{1}{\Delta x}$), while its definition in 3D can be more complex, especially in non-uniform grids. In the MPC model, IAD is defined using the vapour volume fraction gradient:

$$\frac{A_{int}}{V_\Delta} = |\nabla \phi_V|. \tag{13}$$

For complex computational grids, an approximation for Δx is also introduced in the MPC model:

$$\Delta x \approx \sqrt[3]{V_\Delta}. \tag{14}$$

Using improvements of Chen's model, issues with defining r_{Lee} are addressed, but the phase transition location definition is not fully resolved. Thus, two additional conditions were introduced in the proposed model, ensuring phase change occurs only at the interface:

i. evaporation condition:

$$\phi_L > 0,\ T > T_{sat} \tag{15}$$

ii. condensation condition:

$$\phi_V > 0,\ T < T_{sat} \tag{16}$$

For computational stability, these conditions were relaxed in actual simulations to $\phi_L > 10^{-6}$ and $\phi_V > 10^{-6}$. The temperature range where phase change does not occur (transition region) was also extended to $T \in [T_{sat} - 0.5\ \text{K},\ T_{sat}]$.

In the studied cases, both evaporation and condensation (due to high coolant subcooling) occur. The main process is evaporation, as wire superheat is much higher than liquid subcooling. Additionally, condensation is less important due to the density difference between liquid and vapour ($\rho_L : \rho_V \approx 1 : 1000$), meaning evaporation causes changes in volumetric flows three orders of magnitude greater than energy-equivalent condensation processes. Thus, a precise description of evaporation is more crucial than condensation, and in the MPC model, the Chen's approach is used for evaporation, while condensation is modelled using (simpler) Lee's approach. This reduces computational complexity and improves calculation convergence. For the condensation value of 2000 s^{-1} was chosen based on past studies of Lee's model [40]. It should be noted, that as part of the past simulations conducted with the Lee model, the sensitivity of the final results to the condensation intensity factor was also evaluated. The findings confirm that, provided the factor exceeds 1000 s^{-1}, its influence on the solution remains negligible.

A major challenge was the large temperature difference between the wire wall (≈2000 K) and the coolant (≈300 K), leading to intense evaporation. Such processes occur on a very small timescale; in our case, the characteristic evaporation timescale was estimated at 1 μs, while other flow phenomena (like convection and diffusion) occur over 1 s. This disparity introduces large source terms into the conservation equations of two-phase flow (Eq. (5) and (6)), thus adding nonlinearity. Thus, initial calculation steps pose a specific challenge due to large temperature gradients at the interface, necessitated by complex initial condition definitions. To overcome initial convergence issues, r_{MPC} is limited in the MPC model. This allows that, in early calculation stages, MPC acts like Lee's model, transitioning fully to Chen's evaporation description in the developed solution phase. This prevents large source terms in early stages and enabled accurate evaporation description in developed solutions. The r_{max} limit is estimated based on Eq. (12) for r_{Chen}, assuming water's saturation properties and a vapour volume fraction of 0.5. Grid parameters (Δx, IAD) were estimated based on cell size in expected interface regions, and the wire wall temperature was used for T in the estimate. In our simulations, r_{max} was assumed to be 50,000 s^{-1}

To summarize, the final form of the MPC model is given by the following prescription:

$$S_V = r_{MPC}\ \phi_{MPC}\ \rho_{MPC} \frac{T - T_{sat}}{T_{sat}},$$

$$S_h = \ -h_{LV}\ S_V, \tag{17}$$

where r_{MPC}, ϕ_{MPC} and ρ_{MPC} are defined as follows:

- evaporation (condition: $\phi_L > 10^{-6}\ \wedge T > T_{sat}$):

$$\phi_{MPC} = \phi_L,$$

$$\rho_{MPC} = \rho_L,$$

$$r_{MPC} = \min\left(\frac{k_L\ c_{p,L}\ T_{sat}}{\rho_L\ h_{LV}\ \sqrt[3]{V_\Delta}\ (0,5 + 0,5\phi_L)} |\nabla \phi_V|,\ r_{max}\right), \tag{18}$$

- transition region (condition: $T \in [T_{sat} - 0,5\ \text{K},\ T_{sat}]$):

$$r_{MPC} = 0, \tag{19}$$

- condensation (condition: $\phi_V > 10^{-6}\ \wedge\ T < T_{sat} - 0,5$ K):

$$\phi_{MPC} = \phi_V,$$

$$\rho_{MPC} = \rho_V,$$

$$r_{MPC} = 2000\ s^{-1}. \tag{20}$$

The model was realised in the ANSYS Fluent using User Defined Functions (UDFs) [39].

The verification of UDF codes and validation, focusing on the precision of the phase change modelling, were already conducted against the analytical solution of the classic Stefan problem, and is hereafter summarized for completeness [30]. The problem describes the time evolution of the boundary between two phases undergoing a phase change. In this case, we observed the movement of the free boundary between saturated liquid and overheated vapour. It was estimated that the accuracy of MPC model is 2.5 % compared to analytical solution [30]. The calculated time evolution of the interface is shown in Fig. 3a.

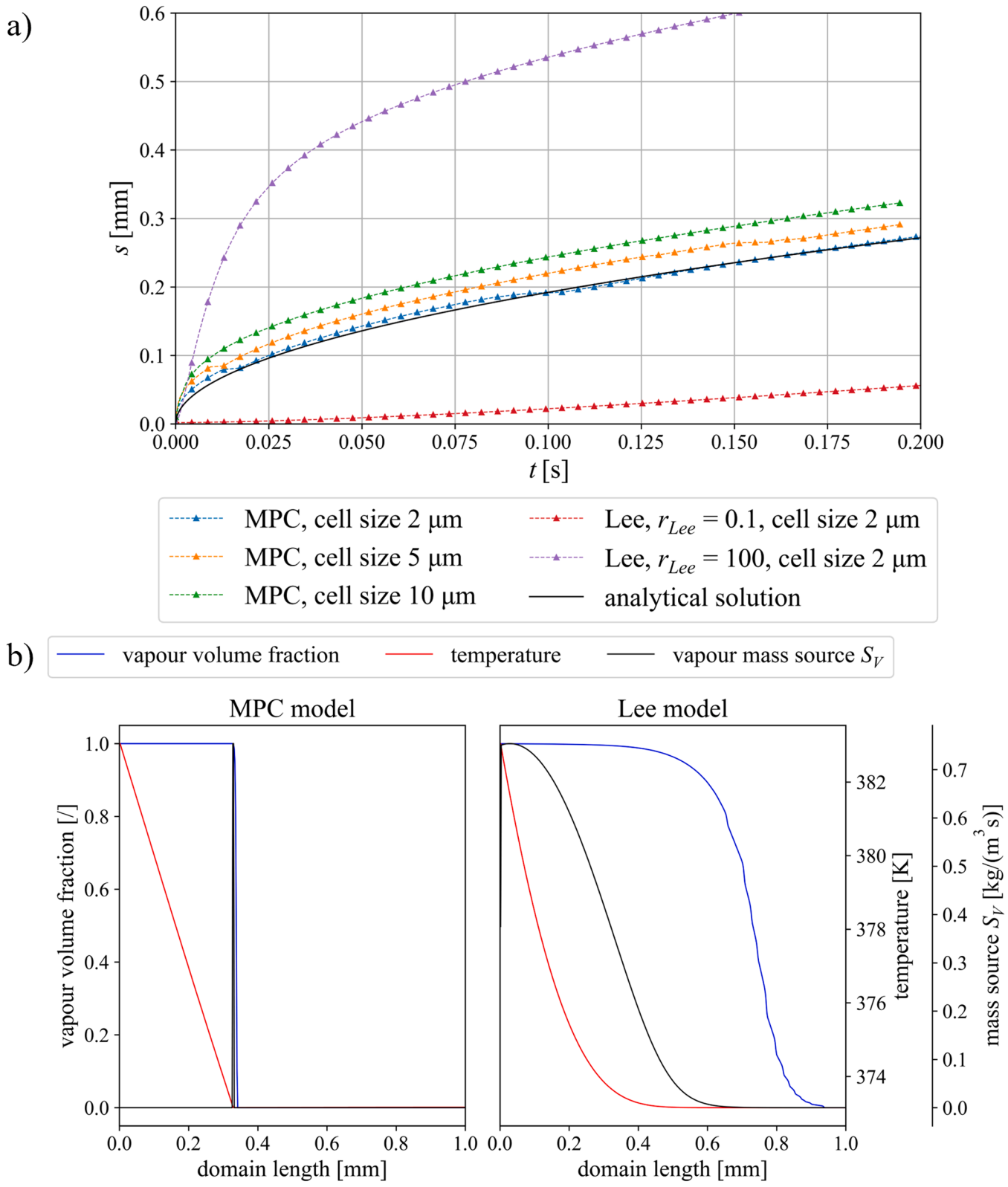

Fig. 3. Time evolution of the interface (recreated based on [30]) – comparison between MPC and Lee model with the analytical solution of Stefan problem (a); Vapour volume fraction, vapour mass source and temperature profile – comparison between solution of MPC and Lee model (b).

The temperature profile and interface and mass source position are shown in Fig. 3b The MPC model displays the characteristics of the Chen model, maintaining sharp interface and no smearing of the mass source at the interface, representing a significant improvement to the Lee model.

3.3. Computational domain, numerical methods and simulation setup

The computational domain, numerical methods, and simulation setup were adopted from our preliminary study [40]. For completeness of this study a concise description is again provided in the following paragraphs.

The computational setup is a representation of the TREPAM experiments. Due to the large temperature difference between the subcooled water T_∞ and the hot wire T_w, variable properties dependent on the local temperature were used. Vapour thermal conductivity k_V, vapour density ρ_V, vapour specific heat at constant pressure $c_{p,V}$, vapour dynamic viscosity μ_V and liquid dynamic viscosity μ_V were defined as polynomial based on [35] and applying [46]. Accurate vapour phase properties were defined between the prescribed boundaries T_{sat} and T_w. Similarly, the liquid phase properties were defined between T_∞ and T_{sat}. However, during numerical iterations, the temperatures in the domain can exceed prescribed boundaries and variable properties yield to non-physical results, therefore beyond the boundaries constant properties were set. Similarly, the surface tension coefficient was defined based on IAPWS R1–76 (2014) [47]. The remaining properties of the liquid phase were assumed as constant and were estimated at the temperature $T_L = (T_{sat} + T_\infty)/2$.

The estimated film thickness was used to define the initial condition for the steady-state simulation and to determine the appropriate size of the mesh cells in the vapour film. All thermodynamic properties used in the estimation were evaluated at the film temperature $T_V = (T_{sat} + T_w)/2$ and $T_L = (T_{sat} + T_\infty)/2$ for the vapour and the liquid phase, respectively.

Assuming a vapour film is thin compared to the wire diameter, a predominant heat transport mechanism is conduction, hence the convective heat transfer can be neglected. The initial thickness of the vapour film δ_V can then be estimated from the measured heat flux q_w [14] with:

$$\delta_V = k_V \frac{(T_w - T_{sat})}{q_w} \tag{21}$$

The size of the computational domain was estimated by analysing digital photograph (see Fig. 1) of the phenomenon captured in the TREPAM experimental setup [14]. The entire phenomenon was intended to be captured within the domain, along with a minor section of the free flow, where no significant flow phenomena were anticipated.

Mesh was designed according to δ_V prescribed by Eq. (21) for a given case. Fig. 4 shows a 2D rectangular computational domain (36 D × 20 D) with a solid circular fragment (wire) at the origin. The domain is bounded by five boundary zones of three types: velocity inlet (inlet, far-field top, far-field bottom), pressure outlet (outlet) and wall boundary (wire wall). For turbulence boundary conditions we assumed the default values recommended by Fluent [37].

Block-structured body fitted C—H type mesh with hexahedral cells was used. To better resolve physics in the vapour film additional block was added, i.e., the estimated vapour film zone. Computational cells in the film zone were uniformly distributed in radial direction. Cells around the film zone were then appropriately clustered considering the cell growth factor less than 1.2. Details of mesh configurations used in the simulations are presented in Table 2.

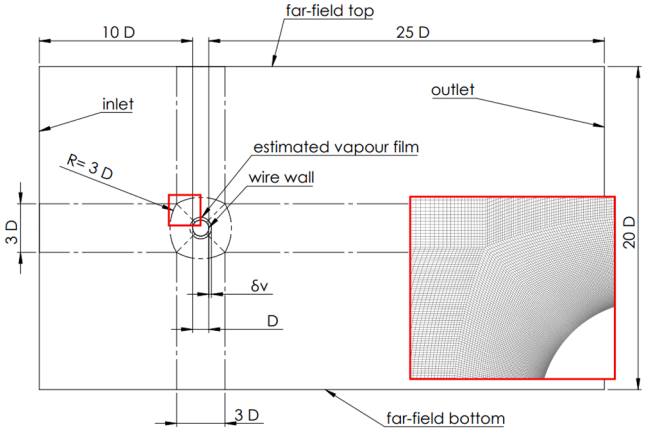

Fig. 4. Sketch of the block-structured domain used in simulations, with a detailed view of the mesh around the wire.

Table 2
Details of mesh configuration.

Case number	D[μm]	Est. δ_V[μm]	Cells in δ_V (radial dir.)	Total cells
54	96	16	28	$1.06{\cdot}10^5$
53	100	10	28	$1.06{\cdot}10^5$
55	99	17	28	$1.06{\cdot}10^5$
61	47	19	20	$6.31{\cdot}10^4$

Simulations were performed employing either the Lee model or the MPC model, with the same mesh used for individual case. In the initial steps of our simulations, there were significant discrepancies between the physical model, boundary, and initial conditions, leading to numerical instability. To enhance the initial solution when employing the Lee model, each case was initially calculated as steady-state. The steady-state simulations were followed by the transient simulations. In simulations with the MPC model, issues with initial conditions were addressed by utilizing solutions derived from the Lee model with $r_{Lee} = 1000$ and progressively increasing the r_{max} values.

In the steady-state simulations, the coupled algorithm with pseudo-transient relaxation [39] was used for pressure-velocity coupling. In the transient simulation the pressure-velocity coupling was done by the SIMPLE algorithm [48]. A second-order upwind scheme was used for spatial discretization of all conservation equations. It should be noted that in the initial calculation steps, a power law scheme [39] was helpful to improving stability and convergence of simulation. Transient simulations of all cases reached a quasi-steady condition and ran well over 100 characteristic time units $\frac{D}{U_\infty}$.

4. Results with discussion

The results of the numerical investigation of the TREPAM experiments [14], conducted using the MPC and Lee models, are presented herein. The adequacy of the simulations was assessed based on the following criteria:

i. fluctuations and the average heat flux between the wire wall and the surrounding fluid q_w,
ii. the ability to maintain the correct location of phase change,
iii. the ability to maintain sharpness of the interfacial surface,
iv. velocity conditions and
v. the distribution of the temperature field across the domain.

4.1. Average heat flux

The first criterion used to evaluate the accuracy of our model was the value of $q_{w,MPC}$ averaged over Δt. Size of $\Delta t = 5 f_s^{-1}$ was estimated from the analogy with the single-phase cross flow over the cylinder, where the shedding frequency is defined by Strouhal number St as:

$$f_s = \mathrm{St}\frac{U_\infty}{D}.$$

Empirical correlation used to predict St applicable to the presented cases is formulated as [12]:

$$\mathrm{St} = 0.198\left(1 - \frac{19.7}{\mathrm{Re_L}}\right).$$

The results, presented in Table 3, compare the final outcome obtained with the model parameter r_{max} set to 50,000 s^{-1} and an intermediate result with r_{max} set to 10,000 s^{-1}.

Overall, the results demonstrate good agreement with experimental data for most cases, generally remaining within or near the experimental

Table 3
Simulation results using the MPC model – $q_{w,MPC}$.

case	r_{max} $[s^{-1}]$	$q_{w,MPC}$ $\left[\frac{MW}{m^2}\right]$	$q_{w,exp}$ $\left[\frac{MW}{m^2}\right]$	$e_{q,r}$ [%]	relative change r_{max} [%]	relative change $q_{w,MPC}$ [%]	note
54	10,000	23.5	18	30.8	400	4.70	base. case
	50,000	22.4		24.6			
53	10,000	15.4	14	9.9	400	1.10	lower T_w
	50,000	15.5		11.1			
55	10,000	16.8	9.0	87.0	400	14.9	lower ΔT_{sub}
	50,000	19.3		114.9			
61	10,000	20.7	16	29.5	–	–	lower v_∞

uncertainty range of 20 % [14]. An exception is Case 55, which is closest to saturation conditions, where the error exceeded 100 %. While this error is significantly higher than in other cases, it is consistent with expectations due to the complexity of the physical phenomena and the limitations inherent in the numerical models used. It is also noteworthy that a similar level of uncertainty (scatter) was observed when TREPAM results were compared with correlations derived from the Epstein-Hauser model [16].

The simulation of case 61 encountered significant convergence issues and resulted in unphysical solutions when using $r_{max} = 50,000$. The most likely cause of this behaviour is that low v_∞ increases the non-linearities in the conservation equations, which, in turn, result in convergence difficulties [30].

A comparable level of accuracy in predicting q_w was achieved in simulations using the Lee model in our previous study [40], provided the model parameter r_{Lee} was set above the value of 1600 s^{-1}. However, the findings of the previous study revealed a strong dependence of the simulated q_w on the model parameter r_{Lee} in the Lee model, where even a slight variation in r_{Lee} could lead to a doubling of q_w [40]. In contrast, a 400 % increase in the parameter r_{max} in the MPC model led to a variation in q_w of less than 15 %. This demonstrates a key advantage of the MPC model, characterized by its significantly lower sensitivity of q_w to r_{max}, indicating greater numerical stability and robustness compared to the Lee model.

Fig. 5 presents the transient evolution of q_w in the simulations of baseline case 54 using the MPC model ($r_{max} = 50,000$ s^{-1}) and the Lee model. The figure also indicates the averaged $q_{w,exp}$ measured in the TREPAM apparatus [14]. The comparison shows that the MPC model produces significantly smaller fluctuations in q_w compared to the Lee model. This suggests a fundamentally different heat transfer dynamics and more stable operating conditions with the MPC model, which align more closely with expectations and experimental data. Similar observations were consistently made across all the considered cases.

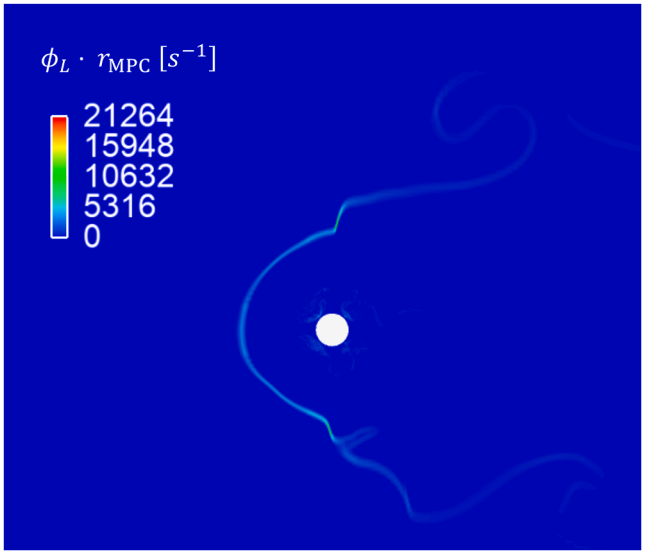

Fig. 6. The phase transfer intensity factor r_{MPC} filtered by ϕ_L in the simulation of Case 54 at $t = 62.93$ ms.

4.2. Phase change localization and flow dynamics

To evaluate how well model determines the location of the phase change, we investigated the fields of the evaporation intensity factor r_{MPC} within the domain. It was observed that r_{MPC} is not homogeneous throughout the domain, which more accurately captures the real physics of the evaporation process. This becomes especially apparent when the term is filtered using the volume fraction of the liquid phase ϕ_L, as shown in Fig. 6. The product $\phi_L \cdot r_{MPC}$ serves as a filter for phase change

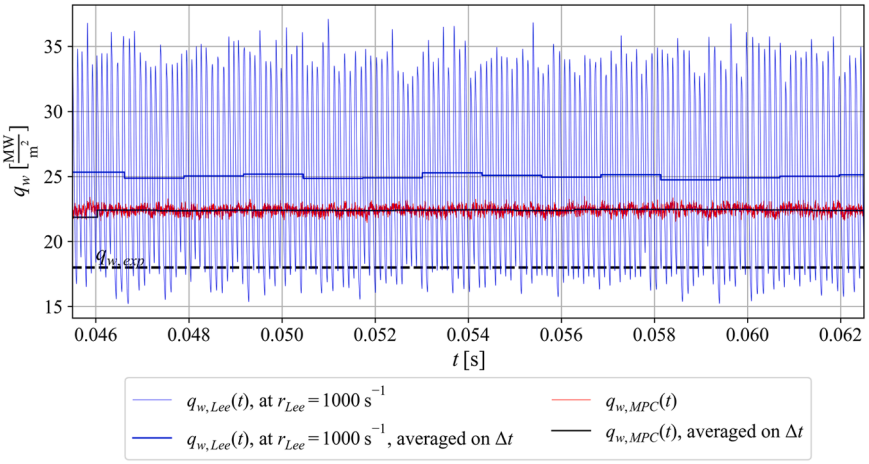

Fig. 5. The transient evolution of q_w for Case 54 – a comparison between the Lee model and the MPC model.

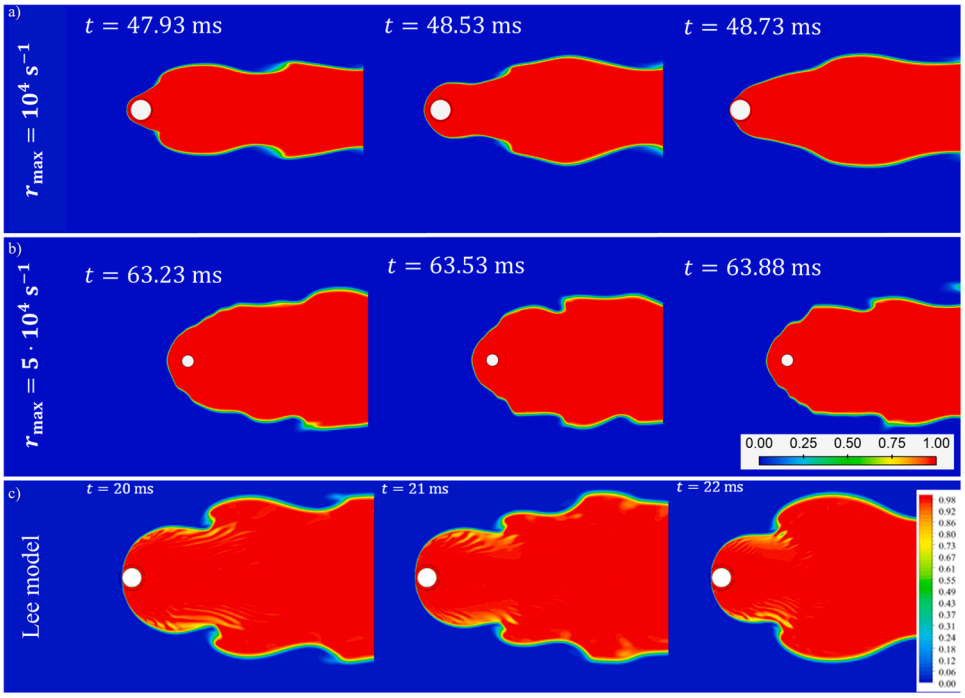

Fig. 7. The transient evolution of the volume vapour fraction ϕ_V for Case 54, simulated using: a) MPC model and $r_{max} = 10,000$ s^{-1}; b) MPC model and $r_{max} = 50,000$ s^{-1}; c) Lee model $r_{Lee} = 1000$ s^{-1} [40].

(evaporation) implemented in the governing equation in the MPC model (Eq. (17)).

The analysis of the results has also confirmed that the MPC model provides an improved ability to maintain the sharpness of the liquid-vapour interface. Additionally, in contrast to the simulations conducted with the Lee model (Fig. 7c), no numerical artefacts were observed in the simulations performed using the MPC model. This is illustrated in Fig. 7a and Fig. 7b, which show the transient evolution of the vapour fraction ϕ_V for the baseline Case 54, simulated using the MPC model. Fig. 7a shows an intermediate result with $r_{max} = 10,000$ s^{-1}, while the Fig. 7b row depicts the final result with $r_{max} = 50,000$ s^{-1}.

The overall flow structure in both cases is similar and aligns with the shape observed in simulations using the Lee model with $r_{Lee} \geq 1000$ [40]. This similarity, shown in the Fig. 7c, is characterized by a symmetric, bubbling vapour wake. On the other hand, more detailed comparison between intermediate result ($r_{max} = 10,000$ s^{-1}) and final result ($r_{max} = 50,000$ s^{-1}) reveals differences in the shape of the vapour film near the wire and the width of the vapour wake, indicating distinct flow dynamics within the vapour phase.

These differences become more pronounced when comparing the velocity fields within the vapour film. Fig. 8 shows the velocity vector fields obtained from simulations using the MPC model, including an intermediate result for $r_{max} = 10,000$ s^{-1}. The results indicate that the more intense evaporation predicted by the MPC model ($r_{max} = 50,000$ s^{-1}) leads to the formation of secondary flows – vortices within the vapour film, which significantly influence the heat transfer mechanism.

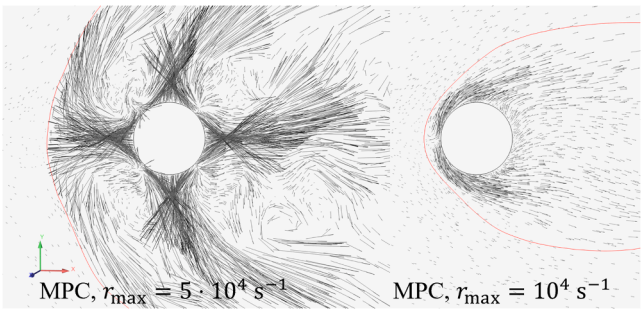

Fig. 8. Comparison of velocity vector fields for Case 54 in simulations with the MPC model; the interface (isoline $\phi_V = 0.5$) is highlighted in red.

These secondary flows affect the intensity of evaporation, represented by the source term S_V (Eq. (6)), and the temperature distribution, as shown in Fig. 9. Consequently, they also shape the heat flux profile from the wire wall (shown in Fig. 10), where heat transfer is most intense at evaporation sites, approximately at 45 °, 135 °, 225 °, and 315 °.

The vortices observed within the vapour film could be attributed to numerical artefacts arising from model assumptions and approximations, particularly due to evaporation spots visible in Fig. 9a. As the VOF approach treats liquid and vapour as immiscible phases separated by a sharp interface, phase change should be confined to that interface. Consequently, evaporation within the liquid bulk or condensation within the vapour bulk is not consistent with the model formulation.

However, it cannot be excluded that the observed flow behaviour could also indicate to the following physical phenomena. The vortical structures suggest the presence of secondary flows within the vapour film. These flows may lead to the formation of wet vapour regions that subsequently dry, superheat, and expand, producing vapour jets impinging on the interface, where cooling and partial rehydration occur. The vapour then recirculates back towards regions of high evaporation intensity, as seen on Fig. 9a. While this mechanism is physically plausible, the simulations presented herein do not allow definitive confirmation.

To assess the robustness of the observed patterns, simulations were repeated on two successively refined meshes. One with twice and another with four times the original mesh density. The vortical structures appeared in both cases. Nonetheless, the additional simulations and available experimental data do not allow full confirmation of the flow behaviour.

Further work is necessary to confirm the physical relevance of these flow structures. In particular, detailed experimental investigations and a comprehensive numerical sensitivity analysis are essential. Key parameters requiring further study include domain size, mesh resolution and

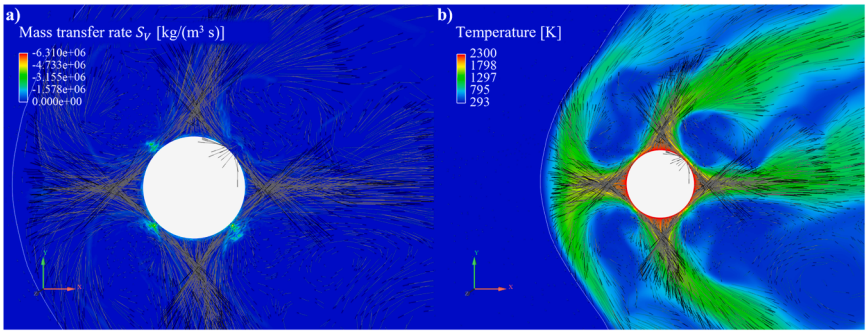

Fig. 9. Contours of mass transfer rate S_V (a) and temperature field (b) in simulation of Case 54 using the MPC model; the interface (isoline $\phi_V = 0.5$) is marked in white.

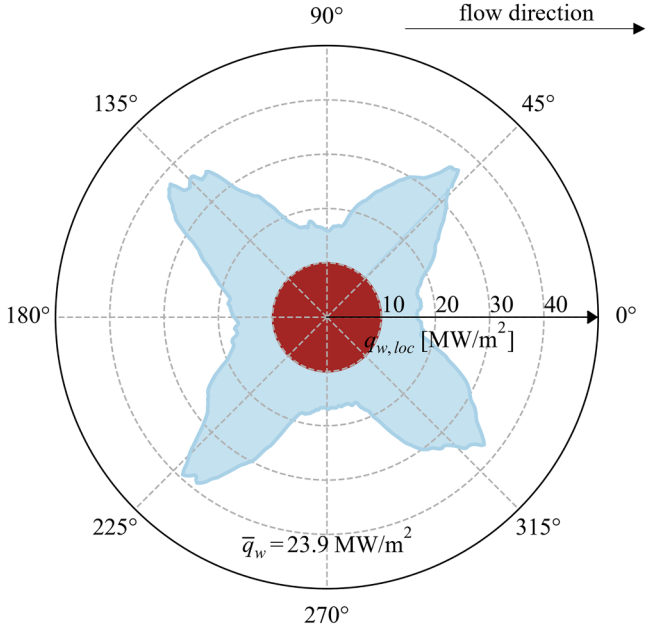

Fig. 10. Instantaneous heat flux profile from the wire wall in polar coordinates for case 54 at time 63.61 ms (MPC model, $r_{max} = 50,000\ s^{-1}$).

structure, boundary conditions, and turbulence modelling. The 2D domain simplification may also artificially enhance certain flow phenomena by limiting out-of-plane dissipation.

Although full validation of the MPC model under such conditions remains outside the scope of this work, the results highlight that flow phenomena within the vapour film, often neglected in prior studies [10, 27], most probably importantly affect the heat and mass transfer mechanisms.

5. Conclusions

The presented study investigated film boiling around a melt particle in a subcooled convective flow, focusing on numerical simulations based on the TREPAM experiments (CEA, France). These experiments replicate conditions encountered during fuel-coolant interactions, subjecting the simulations to extreme conditions, including large subcooling (over 80 K) and substantial wall overheating (above 2000 K). This study is among the first attempts to simulate such conditions using a fully two-phase CFD approach in a 2D geometry.

The main contribution of this work are the proposed modifications to a phase-change model combining the physical formulation of the Chen model with the numerical robustness of the Lee model. The proposed model introduces a locally defined, physically based phase-change intensity factor, capped by a stability limiter, enabling convergence in highly non-linear conditions, typical for energetic solid-coolant interaction. Unlike the original Lee model, proposed approach does not rely on a globally constant intensity factor and significantly reduces sensitivity to user-defined parameters.

Simulations demonstrated that proposed approach improves the prediction of heat flux magnitude as well as oscillations compared to standard Lee model. It provides sharper interface resolution and more accurate localisation of the phase-change zone. Furthermore, the results suggest that flow structures in the vapour film, though still subject to numerical uncertainty, may significantly influence heat transfer mechanisms, highlighting a need for further numerical and experimental studies.

Despite the improvements, the proposed phase-change modelling approach requires further validation. Future work should focus on evaluating the impact of turbulence modelling, domain dimensionality, and grid resolution. The current lack of detailed experimental data, especially on vapour film structure and interfacial transport, remains a key limitation.

In summary, proposed modifications represents a general enhancement to existing phase-change models, enabling physically consistent and numerically stable simulation of multiphase heat and mass transfer. While its advantages are particularly evident under extreme conditions, such as those encountered in energetic solid-coolant interactions, the model is not limited to the specific geometry or conditions of the simulated TREPAM experiments. Its formulation is applicable to non-uniform 2D and 3D grids and various fluids. The approach thus enhances the predictive capability of CFD tools for complex multiphase systems, supporting future model development and safety analysis in energy and nuclear engineering.

Declaration of generative AI in the writing process

During the preparation of this work the authors used Chat GPT-4 and DeepL to improve readability and language. After using this tool/service, the authors reviewed and edited the content as needed and take full responsibility for the content of the publication.

CRediT authorship contribution statement

Mihael Boštjan Končar: Writing – original draft, Visualization, Software, Methodology, Conceptualization. **Matej Tekavčič:** Writing – review & editing, Supervision, Methodology, Conceptualization. **Mitja Uršič:** Writing – review & editing, Supervision, Methodology, Conceptualization. **Mihael Sekavčnik:** Writing – review & editing.

Declaration of competing interest

The authors declare that they have no known competing financial interests or personal relationships that could have appeared to influence the work reported in this paper.

Acknowledgments

The Jožef Stefan Institute authors acknowledge the financial support from the Slovenian Research Agency (research core funding No. P2–0026) and from the state budget by the Slovenian Research Agency and the Slovenian Nuclear Safety Administration (project No. V2–2375). The authors from the Faculty of Mechanical Engineering, University of Ljubljana gratefully acknowledge the financial support provided by German Academic Exchange Service (*"Deutscher Akademischer Austauschdienst"*, DAAD), PhD research grant No. 57693451.

Data availability

Data will be made available on request.

References

[1] C. Journeau, L. Aufore, L. Berge, C. Brayer, N. Cassiaut-Louis, N. Estre, F. Payot, P. Piluso, J.-C. Prele, S. Singh, M. Zabiégo, E. Pluyette, F. Serre, B. Teisseire, Corium-sodium and Corium-water fuel-coolant-interaction experimental programs for the PLINIUS2 prototypic Corium platform, Nucl. Technol. 205 (2019) 239–247, https://doi.org/10.1080/00295450.2018.1479580.

[2] M.L. Corradini, B.J. Kim, M.D. Oh, Vapor explosions in light water reactors: a review of theory and modeling, Progress in Nuclear Energy 22 (1988) 1–117, https://doi.org/10.1016/0149-1970(88)90004-2.

[3] OECD/NEA, OECD Research programme on fuel-coolant interaction: steam explosion Resolution for nuclear applications – SERENA; final report, 2007.

[4] A. Seshadri, K. Shirvan, Quenching heat transfer analysis of accident tolerant coated fuel cladding, Nuclear Eng. Design 338 (2018) 5–15, https://doi.org/10.1016/j.nucengdes.2018.07.020.

[5] H. Lee, D.E. Kim, J. Park, H. Kim, Effects of liquid subcooling on droplet-wall collision heat transfer in film boiling, Exp. Therm. Fluid. Sci. 132 (2022) 110571, https://doi.org/10.1016/j.expthermflusci.2021.110571.

[6] A. Luketahanlin, A review of large-scale LNG spills: experiments and modeling, J. Hazard. Mater. 132 (2006) 119–140, https://doi.org/10.1016/j.jhazmat.2005.10.008.

[7] P. Moitra, I. Sonder, G.A. Valentine, The role of external water on rapid cooling and fragmentation of magma, Earth. Planet. Sci. Lett. 537 (2020) 116194, https://doi.org/10.1016/j.epsl.2020.116194.

[8] C. Liu, T.G. Theofanous, Film Boiling on Spheres in Single- and Two-Phase Flows, 2000, https://doi.org/10.2172/764210.

[9] A. Inoue, Y. Fujii, S. Lee, Studies on transient film boiling heat transfer from thin wires penetrating through liquid interface, in: Proceedings of the International Seminar on Vapor Explosions and Explosive Eruptions, Sendai, Japan, 1997, pp. 123–130.

[10] E. de Malmazet, G. Berthoud, Convection film boiling on horizontal cylinders, Int. J. Heat. Mass Transf. 52 (2009) 4731–4747, https://doi.org/10.1016/j.ijheatmasstransfer.2009.03.065.

[11] V.K. Dhir, G.P. Purohit, Subcooled film-boiling heat transfer from spheres, Nuclear Eng. Design 47 (1978) 49–66, https://doi.org/10.1016/0029-5493(78)90004-3.

[12] H. Honda, H. Takamatsu, H. Yamashiro, S. Kobayashi, Heat-transfer characteristics during rapid quenching of a thin wire in water, Heat Trans. - Japanese Research 21 (1992) 773–791.

[13] M. Epstein, G.M. Hauser, Subcooled forced-convection film boiling in the forward stagnation region of a sphere or cylinder, Int. J. Heat. Mass Transf. 23 (1980) 179–189, https://doi.org/10.1016/0017-9310(80)90195-7.

[14] G. Berthoud, L.G. D'Aillon, Film boiling heat transfer around a very high temperature thin wire immersed into water at pressure from 1 to 210 bar: experimental results and analysis, Int. J. Thermal Sci. 48 (2009) 1728–1740, https://doi.org/10.1016/J.IJTHERMALSCI.2009.01.012.

[15] G. Berthoud, Use of the TREPAM hot wire quenching test results for modelling heat transfer between fuel and coolant in FCI codes, Nuclear Eng. Design 239 (2009) 2908–2915, https://doi.org/10.1016/j.nucengdes.2009.08.031.

[16] R. Meignen, S. Picchi, J. Lamome, B. Raverdy, S.C. Escobar, G. Nicaise, The challenge of modeling fuel–coolant interaction: part I – Premixing, Nuclear Eng. Design 280 (2014) 511–527, https://doi.org/10.1016/j.nucengdes.2014.08.029.

[17] R. Meignen, D. Magallon, K.-H. Bang, G. Berthoud, S. Basu, M. Buerger, M. Buck, M.L. Corradini, H. Jacobs, O. Melikhov, M. Naitoh, K. Moriyama, R. Sairanen, J.-H. Song, N. Suh, T.G. Theofanous, Comparative review of FCI computer models used in the OECD-SERENA program. Advances in Nuclear Power Plants 2005, American Nuclear Society (ANS), United States, 2005, pp. 411–423.

[18] M. Uršič, R. Meignen, M. Leskovar, Analysis of film boiling heat transfer during fuel-coolant interaction, Int. J. Heat. Mass Transf. 107 (2017) 622–630, https://doi.org/10.1016/j.ijheatmasstransfer.2016.11.055.

[19] C.R. Kharangate, I. Mudawar, Review of computational studies on boiling and condensation, Int. J. Heat. Mass Transf. 108 (2017) 1164–1196, https://doi.org/10.1016/j.ijheatmasstransfer.2016.12.065.

[20] F. Gibou, L. Chen, D. Nguyen, S. Banerjee, A level set based sharp interface method for the multiphase incompressible Navier-Stokes equations with phase change, J. Comput. Phys. 222 (2007) 536–555, https://doi.org/10.1016/j.jcp.2006.07.035.

[21] R.W. Schrage, A Theoretical Study of Interphase Mass Transfer, Columbia University Press, New York Chichester, West Sussex, 1953, https://doi.org/10.7312/schr90162.

[22] W.H. Lee, Pressure iteration scheme for two-phase flow modeling., Multi-phase transport: fundamentals, reactor safety, Applications 1 (1980) 407–431, https://doi.org/10.1142/9789814460286_0004.

[23] Z. Liu, B. Sunden, J. Yuan, Vof modeling and analysis of filmwise condensation between vertical parallel plates, Heat. Transf. Res. 43 (2012) 47–68, https://doi.org/10.1615/HeatTransRes.2012004376.

[24] S. Petrovic, T. Robinson, R.L. Judd, Marangoni heat transfer in subcooled nucleate pool boiling, Int. J. Heat. Mass Transf. 47 (2004) 5115–5128, https://doi.org/10.1016/J.IJHEATMASSTRANSFER.2004.05.031.

[25] P. Arlabosse, L. Tadrist, H. Tadrist, J. Pantaloni, Experimental analysis of the heat transfer induced by thermocapillary convection around a bubble, Volume 122, Issue 1, Pages 66 - 73 122 (2000) 66–73. https://doi.org/10.1115/1.521438.

[26] R. Meignen, P. Piluso, N. Rimbert, Outcomes of the French ICE project on fuel coolant interaction, in: 17th International Topical Meeting on Nuclear Reactor Thermal Hydraulics, NURETH-17, 2017, pp. 1–16.

[27] G. Berthoud, Use of the TREPAM hot wire quenching test results for modelling heat transfer between fuel and coolant in FCI codes, Nuclear Eng. Design 239 (2009) 2908–2915, https://doi.org/10.1016/j.nucengdes.2009.08.031.

[28] S.E. Yakush, N.S. Sivakov, Numerical modeling of high-temperature melt droplet interaction with water, Ann. Nucl. Energy 185 (2023) 109718, https://doi.org/10.1016/j.anucene.2023.109718.

[29] G. Chen, T. Nie, X. Yan, An explicit expression of the empirical factor in a widely used phase change model, Int. J. Heat. Mass Transf. 150 (2020) 119279, https://doi.org/10.1016/j.ijheatmasstransfer.2019.119279.

[30] M.B. Končar, M. Tekavčič, M. Uršič, Application of enhanced phase-change model for simulation of film boiling around a cylinder, in: I. Jenčič (Ed.), Proceedings of the 31. Conference Nuclear Energy for New Europe 2022, Nuclear Society of Slovenia, Portorož, 2022, 414.1-414.8.

[31] I. Huhtiniemi, D. Magallon, H. Hohmann, Results of recent KROTOS FCI tests: alumina versus corium melts, Nuclear Eng. Design 189 (1999) 379–389, https://doi.org/10.1016/S0029-5493(98)00269-6.

[32] R.-Q. Duan, S. Koshizuka, Y. Oka, Numerical and theoretical investigation of effect of density ratio on the critical Weber number of droplet breakup, J. Nucl. Sci. Technol. 40 (2003) 501–508, https://doi.org/10.1080/18811248.2003.9715384.

[33] H.K. Versteeg, W. Malalasekera, An Introduction to Computational Fluid Dynamics, 2nd ed., Pearson Education Limited, Harlow, 2007.

[34] R. Karwa, Heat and Mass Transfer, 2nd Edition, Springer, Singapure, 2020.

[35] I.H. Bell, J. Wronski, S. Quoilin, V. Lemort, Pure and pseudo-pure fluid thermophysical property evaluation and the open-source thermophysical property library CoolProp, Ind. Eng. Chem. Res. 53 (2014) 2498–2508, https://doi.org/10.1021/ie4033999.

[36] R.L. Panton, Chapter 14.6: flow around a circular cylinder. Incompressible Flow, John Wiley & Sons Inc., Hoboken, 2013, pp. 346–362.

[37] M. Uršič, M. Leskovar, R. Meignen, S. Picchi, J.A. Zambaux, Fuel coolant interaction modelling in sodium cooled fast reactors, in: EUROSAFE: Proceedings of EUROSAFE Forum, München, 2016, pp. 113–128.

[38] A. Faghri, Y. Zhang, Transport Phenomena in Multiphase Systems, Elsevier Inc., Oxford, 2010.

[39] ANSYS Inc., ANSYS Academic Research, Fluent 19 R1, Help System, ANSYS Fluent Theory Guide, 2019.

[40] M.B. Končar, M. Tekavčič, M. Uršič, Film boiling simulation around cylinder with ANSYS fluent, in: L. Cizelj, M. Tekavčič (Eds.), Proceedings of the 30. Conference Nuclear Energy for New Europe 2021, Nuclear Society of Slovenia, Bled, 2021, 619.1-619.8.

[41] M. Tekavčič, Ž. Kogovšek, M. Uršič, M. Leskovar, Simulations of heat and mass transfer around circular core fragment in sodium coolant, in: B. Smodiš, N. Udir, A. Jazbec, M. Rosman (Eds.), Proceedings of the 28. Conference Nuclear Energy for New Europe 2019, Nuclear Society of Slovenia, Portorož, 2019, 408.1-408.11.

[42] C.W. Hirt, B.D. Nichols, Volume of fluid (VOF) method for the dynamics of free boundaries, J. Comput. Phys. 39 (1981) 201–225, https://doi.org/10.1016/0021-9991(81)90145-5.

[43] F.R. Menter, M. Kuntz, R. Langtry, Ten years of industrial experience with the SST turbulence model, in: K. Hanjalic, Y. Nagano, M. Tummers (Eds.), Turbulence, Heat and Mass Transfer, 4th Edition, Begell House Inc., Connecticut, 2003, pp. 625–632.

[44] J.U. Brackbill, D.B. Kothe, C. Zemach, A continuum method for modeling surface tension, J. Comput. Phys. 100 (1992) 335–354, https://doi.org/10.1016/0021-9991(92)90240-Y.

[45] X. Yan, G. Chen, An approximation approach for the simulation of vapor-liquid phase change by the volume-of-fluid method, Int. J. Multiphase Flow 136 (2021) 103359, https://doi.org/10.1016/j.ijmultiphaseflow.2020.103359.

[46] C.R. Harris, K.J. Millman, S.J. van der Walt, R. Gommers, P. Virtanen, D. Cournapeau, E. Wieser, J. Taylor, S. Berg, N.J. Smith, R. Kern, M. Picus, S. Hoyer, M.H. van Kerkwijk, M. Brett, A. Haldane, J.F. del Río, M. Wiebe, P. Peterson, P. Gérard-Marchant, K. Sheppard, T. Reddy, W. Weckesser, H. Abbasi, C. Gohlke, T.E. Oliphant, Array programming with NumPy, Nature 585 (2020) 357–362, https://doi.org/10.1038/s41586-020-2649-2.

[47] IAPWS R1-76, Revised release on surface tension of ordinary water substance, (2014).

[48] S.V. Patankar, Numerical Heat Transfer and Fluid Flow, CRC Press, 2018, https://doi.org/10.1201/9781482234213.